GU J Sci 31(1): 251-271 (2018)

Gazi University

Journal of Science

http://dergipark.gov.tr/gujs

Design and Development of the I.T.U. Biped Robot

Zeki Yağız BAYRAKTAROĞLU[1,*], Mesut ACAR[1], Alper GERÇEK[2], Numan Mert TAN[1]

[1]*Istanbul Technical University, Mechanical Engineering Department, Gümüşsuyu 34437, Beyoğlu, Istanbul*

[2]*Altinay Robot Technnologies Inc., Istanbul Industry and Trade Free Zone, 34957, Tuzla, Istanbul*

Article Info

Received: 24/05/2017
Accepted: 25/12/2017

Keywords

Biped robot
Dynamical simulation
Design
Motion control

Abstract

This paper presents the design and construction of a 12-DoF biped walking robot. The kinematics of electrically actuated 6-DoF legs is similar to that of human legs with three DoF at the hip, one at the knee and two at the ankle joints. The mechanical design of the robot was based on dynamical simulations realized in a modular PC environment. Two communicating software were used in order to solve the forward dynamics of the system and to design walking controllers. Forward, backward and lateral walking as well as stair climbing behaviors with up to 6 km/h forward walking speeds have been simulated in order to determine the nominal power rates required at joints. Hip joints are actuated by DC motors coupled to harmonic reducers situated both in joint axes. The actuators driving the knee and ankle joints are situated higher than the respective joint axes and the rotational output motion of DC motors are transmitted to the joints through linear ball-screw mechanisms. Spherical joints are used within the transmission of spatial motion required for the 2-DoF at ankle joints. All joints consist of absolute encoders and 6-axes force/torque transducers are mounted at the ankle joints. The robot is controlled through an embedded industrial PC running real-time operating system. All electronic control hardware including the motor drivers and sensors communicate through CAN bus. The robot's mass without batteries is 55 kg and its height is 142 cm.

1. INTRODUCTION

In the last decades, important technological developments occurred in sensor, actuator, and computer technologies. Humanoid robotics is one of the research fields which exploited these technological developments. Although the construction of human-like machines has been always a desire for mankind, it has only become possible recently at the end of the 20th century. The present section focuses on human-size humanoid and biped robots.

Japan is the leading country in development and construction of humanoid robots. Asimo, a child size humanoid by Honda, is one of the most advanced prototypes with running speed of 6 km/h [1-3]. The HRP series developed by AIST in Japan are also remarkable prototypes with maximum walking speed of 2.5 km/h [4-7]. Waseda University is another leading research center in biped and humanoid robotics where Kato and his team developed the first dynamically balanced biped walking robot WL-10RD [8]. After Kato's pioneering study, humanoid robot prototypes (Wabian) were developed at Waseda University [9]. In Korea, a series of humanoid robot platforms (KHR) were developed.

A maximum walking speed of 1.25 km/h was achieved by KHR-3 prototype [10]. In Germany, the Technical University of Munich (TUM) developed two humanoid prototypes, Johnnie with a walking speed of 2 km/h and Lola [11-14]. A 41-DoF humanoid robot Reem-B developed by Pal Technology Robotics in Spain reaches walking speed of 1.5 km/h [15]. In Turkey, Sabanci University recently introduced SURALP [16], a 29 DoF humanoid prototype.

*Corresponding author, e-mail: zeki.bayraktaroglu@itu.edu.tr

Beside full humanoids, there are also walking biped robots constructed in order to explore dynamics and control of biped walking. Research and development of full humanoid robots is largely based on the analysis and control of humanoid biped locomotion. Biped robots introduced in 1980s at MIT Leg Laboratory are among the pioneer prototypes [17]. Passive walkers were developed at the TU Delft [18]. BIP2000 [19] at INRIA and Robian [20] at LISV in France can be cited among the other biped robots. Although non anthropomorphic, the biped Petman recently introduced by Boston Dynamics exhibits remarkable walking behaviour [21]. A publication by Chevallereau et al. represents a state-of-the-art on bipedal robots [22].

Biped walking is the most fundamental behavior to be accomplished by humanoid robots. There are a great number of published research papers in scientific and engineering literature dealing with modelling and control of biped walking. However, the number of human-size physical prototypes remains limited compared to that of theoretical and computational works achieved on biped walking. Experimental research is an important part for a comprehensive study and a better understanding of human-like biped walking. The aim of the project presented in this paper is to investigate the fundamentals of biped walking through the design and construction of a robot prototype. The robot prototype is serving as an experimental platform for research on biped walking at the Istanbul Technical University (I.T.U.).

A summary of kinematic and dynamic modelling as well as control of biped walking is given in Section 2. The simulation environment is also presented. In Section 3, mechanical design of the biped robot is presented in two successive steps of selection of actuation components and design. Electrical and control system design and related component selection are given in Section 4. First experiments with the biped robot is presented in the final Section with a brief conclusion.

2. MODELING AND SIMULATION OF BIPED WALKING

Research in modelling of humanoid biped walking dates back to early 1970s. Pioneering works of Kato et al. [8,28,29], Raibert [17], McGhee [23,24] and Vukobratovic [25-27] addressed the most fundamental questions related to the modelling and control of biped locomotion. Further contributions of Shih [30-33], Kajita et al. [34-36], Park et al. [10,37,38], Choi et al. [39-41] among many others established a strong theoretical background for the modelling of biped walkers and dynamics of biped walking behavior itself. Preliminary design of the I.T.U. biped robot has already been presented in [42]. This paper presents in detail the entire modelling, design and construction work of the robot.

2.1. Kinematics

The DoFs and basic dimensions of the selected biped structure are shown in Figure 1. Each leg of the model consists of 6 DoF, three at the hip joint, one at knee joint and two at the ankle joint. $\boldsymbol{x}^{(0)}$ and $\boldsymbol{x}^{(1)}$ denote respectively the position vectors of the body center and left foot. $\boldsymbol{R}^{(0)}$ and $\boldsymbol{R}^{(1)}$ represent respectively the transformation matrices describing the orientations of the body center and left foot. The equations of kinematics for the right leg are straightforwardly obtained.

2.1.1. Forward Kinematics

The forward kinematics provides the position and orientation of the feet with respect to the body center in terms of the joint positions. Equations of the forward kinematics of the left leg are written as follows:

$$\boldsymbol{R}^{(1)} = \boldsymbol{R}^{(0)}\boldsymbol{R}_{\boldsymbol{z}}(\theta_1)\boldsymbol{R}_{\boldsymbol{x}}(\theta_2)\boldsymbol{R}_{\boldsymbol{y}}(\theta_3)\boldsymbol{R}_{\boldsymbol{y}}(\theta_4)\boldsymbol{R}_{\boldsymbol{y}}(\theta_5)\boldsymbol{R}_{\boldsymbol{x}}(\theta_6) \tag{1}$$

$$\boldsymbol{x}^{(1)} = \boldsymbol{x}^{(0)} + \boldsymbol{R}^{(0)}\begin{pmatrix}0\\ w_0\\ -h_0\end{pmatrix} + \boldsymbol{R}^{(0)}\boldsymbol{R}_{\boldsymbol{z}}(\theta_1)\boldsymbol{R}_{\boldsymbol{x}}(\theta_2)\boldsymbol{R}_{\boldsymbol{y}}(\theta_3)\begin{pmatrix}0\\ 0\\ -d_1\end{pmatrix} + \boldsymbol{R}^{(0)}\boldsymbol{R}_{\boldsymbol{z}}(\theta_1)\boldsymbol{R}_{\boldsymbol{x}}(\theta_2)\boldsymbol{R}_{\boldsymbol{y}}(\theta_3)\boldsymbol{R}_{\boldsymbol{y}}(\theta_4)\begin{pmatrix}0\\ 0\\ -d_2\end{pmatrix} +$$

$$\boldsymbol{R}^{(1)}\begin{pmatrix} d_4 \\ 0 \\ -d_3 \end{pmatrix} \tag{2}$$

where $\boldsymbol{R_x}(\theta)$, $\boldsymbol{R_y}(\theta)$ and $\boldsymbol{R_z}(\theta)$ are the rotation matrices.

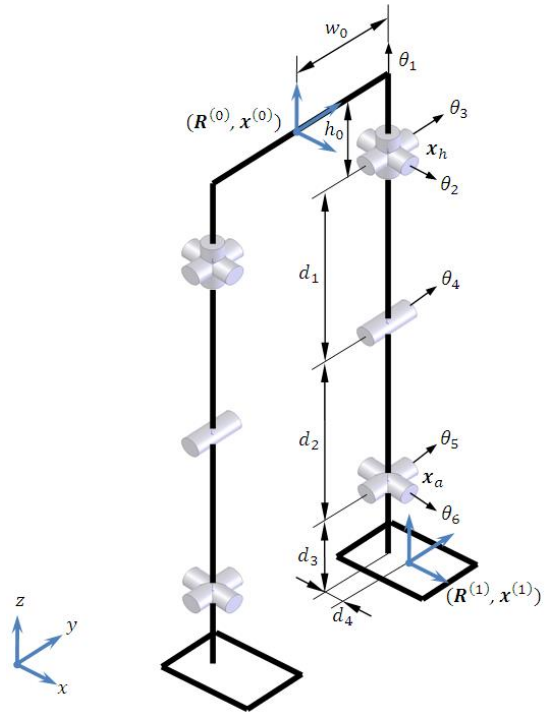

Figure 1. *DoFs and basic parameters of the selected biped structure*

2.1.2. Inverse Kinematics

The inverse kinematics is used for the computation of joint positions satisfying desired relative positions and orientations between the body center and feet. The hip and ankle positions denoted by $\boldsymbol{x}_h$ and $\boldsymbol{x}_a$ in Figure 1 can be expressed as follows:

$$\mathbf{x}_{\mathrm{h}} = \boldsymbol{x}^{(0)} + \boldsymbol{R}^{(0)}\begin{pmatrix} 0 \\ w_0 \\ -h_0 \end{pmatrix} \quad , \quad \mathbf{x}_a = \boldsymbol{x}^{(1)} + \boldsymbol{R}^{(1)}\begin{pmatrix} 0 \\ 0 \\ d_3 \end{pmatrix} \tag{3) , (4}$$

with $(u \quad v \quad w)^T = \left(\boldsymbol{R}^{(1)}\right)^{-1}(\mathbf{x}_h - \mathbf{x}_a)$, θ_4 , θ_5 and θ_6 are obtained as follows:

$$\theta_4 = \cos^{-1}\left(\frac{u^2+v^2+w^2-{d_1}^2-{d_2}^2}{2d_1d_2}\right) \quad , \quad \theta_5 = \sin^{-1}\left(\frac{-{d_1}^2\sin\theta_4}{\sqrt{u^2+v^2+w^2}}\right) - \tan^{-1}\left(\frac{u}{\sqrt{v^2+w^2}}\right) \tag{5) , (6}$$

$$\theta_6 = -\tan^{-1}\left(\frac{u}{w}\right) \tag{7}$$

Rearranging the Eq. (1), θ_3 , θ_2 and θ_1 are obtained as follows:

$$\boldsymbol{R_y}(\theta_3)\boldsymbol{R_x}(-\theta_2)\boldsymbol{R_z}(-\theta_1) = \boldsymbol{R_y}(\theta_4)\boldsymbol{R_y}(\theta_5)\boldsymbol{R_x}(\theta_6)\left(\boldsymbol{R}^{(1)}\right)^{-1}\boldsymbol{R}^{(0)} = \begin{pmatrix} r_{11} & r_{12} & r_{13} \\ r_{21} & r_{22} & r_{23} \\ r_{31} & r_{32} & r_{33} \end{pmatrix}$$

$$\theta_1 = -\tan^{-1}(r_{21}, r_{22}) \quad , \quad \theta_2 = \tan^{-1}\left(r_{23}, \sqrt{{r_{21}}^2 + {r_{22}}^2}\right) \tag{8) , (9}$$

$$\theta_3 = -\tan^{-1}(r_{13}, r_{33}) \tag{10}$$

2.2. Dynamics

Biped walking is a result of periodic motions of the two legs. In the single support phase, the mechanism remains on one foot only while the other one swings between successive steps. The double support phase is the period where both feet are simultaneously in contact with the ground. Along with the assumption of low speed (static) walking, the biped mechanism can be considered as a serial manipulator in single support phase, the lower leg standing for the first link. Therefore, the equations of motion of the biped mechanism can be derived through classical methods used in modelling of industrial manipulators.

Dynamic simulations of the walking mechanism are based on the forward dynamics whose equations are solved by using Msc.Adams® software. Equations of the inverse dynamics are used to apply a model-based control of the system and established by using the Luh-Paul-Walker algorithm [43] based on the iterative Newton-Euler equations.

2.3. Control

Once the desired feet and torso trajectories are determined, the inverse kinematics provides the controller with corresponding desired joint trajectories. The torso trajectory is generated such that the mechanism maintains its walking equilibrium for given feet trajectories and therefore desired Zero Moment Point (ZMP) positions. In the generation of torso trajectory, a linear inverted pendulum model [35,37] is used along with a model predictive algorithm [36,38]. The simulation diagram of the control system is shown in Figure 2, where MPC is the model predictive controller and LIPM the linear inverted pendulum model. Desired feet trajectories and ZMP references are generated off-line.

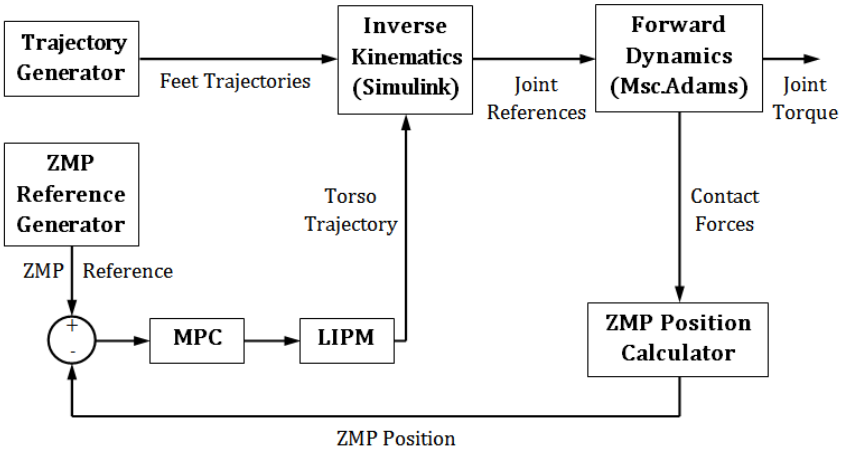

Figure 2. *Simulation diagram*

During walking, the ZMP calculator computes the actual ZMP position by using the contact forces measured in Msc.Adams. Joint references given by the inverse kinematics are transmitted to the Msc.Adams, which in turn computes the joint torque required to track desired references. An example from simulations of forward walking where the desired and computed ZMP trajectories are shown with the footprints is given in Figure 3.

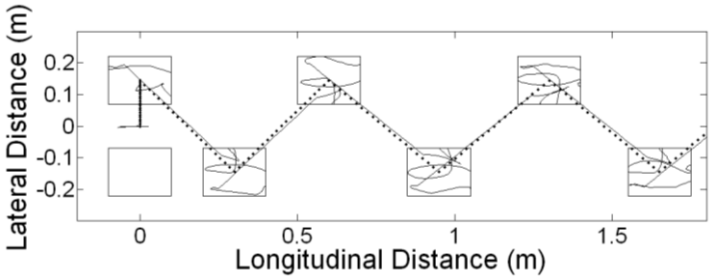

Figure 3. *Desired (dashed) and computed (solid) ZMP trajectories in 1km/h forward walking*

2.4. Simulation Environment

The simulation environment consists of two software running in cooperation under Windows XP® operating system. Communication between software is made through Windows DDE. The Msc.Adams is used to solve the dynamics of biped walking while Simulink® runs the pattern generation algorithms and control laws. The solid model of the robot is designed in SolidWorks® and then exported to Msc.Adams. The simulation program is run in a PC with 1.86 GHz processor and the integration step used in simulations is $5.10^{-4} sec$.

In dynamic simulations, Msc.Adams is provided either with joint positions or with joint torque as reference inputs. The first case corresponds to independent joint control scheme, applied in low speed static walking simulations. In this case, the useful output of simulation is the measured joint torque necessary to achieve the walking behaviour over desired trajectories.

The second case corresponds to computed torque control scheme, applied in higher speed dynamic walking simulations. In this case, the output of interest of the simulation are the resulting motion trajectories and contact forces. Both methods have been applied in simulations of the biped model. Dimensioning of the mechanism is achieved by an iterative process between simulation and redesign.

3. BIPED ROBOT DESIGN

3.1. Dimensioning of the Mechanism

Dimensioning and selection of the actuators and transmissions of the robot is based on the results of the dynamic walking simulations. Since the computed joint torque and velocities define a measure of the required power at each joint, they are the useful outputs of the simulations. Behaviors considered in dynamic simulations include forward, backward and lateral walking, turning right and left and climbing stairs.

3.1.1. Hip Joints

At hip joints, the reduction is between parallel axes and its ratio is given by a constant which is the gear ratio of harmonic drives. In order to obtain the required characteristics for the actuation system including DC motors and harmonic reducers, joint torque and velocities obtained in simulations have been converted to motor torque and velocities. Joint torque and velocities measured at 1 km/h walking speed are shown in Figures 4 and 5. Power reduction from the joints to motors gives the required motor load characteristics. Hip-x motor load characteristic obtained from the simulation outputs of Figures 4 and 5 is given as an example in Figure 6.

Figure 4. *Joint torque (Nm) measured in dynamic walking simulation*

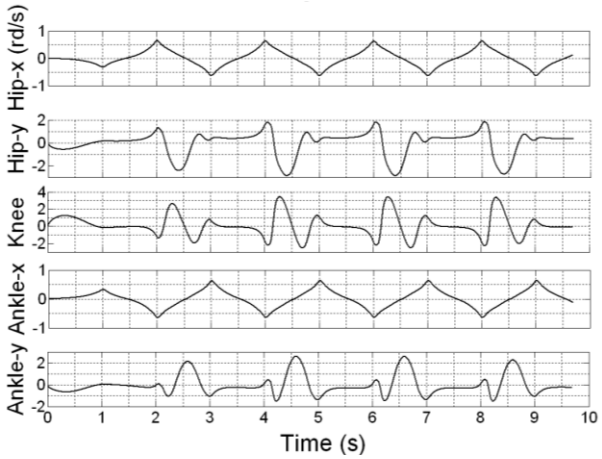

Figure 5. *Joint velocities (rad/s) measured in dynamic walking simulation*

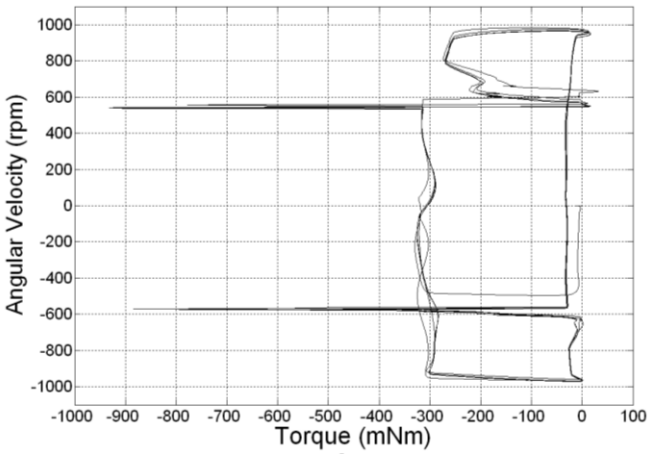

Figure 6. *Hip-x motor load characteristics*

3.1.2. Knee Joints

At the knee and ankle joints, the power transmission occurs between perpendicular rotation axes through ball-screw mechanisms. Therefore, nonlinear algebraic equations have to be solved in order to compute the required motor torque and velocities. The planar knee joint kinematics is described in Figure 7. The motor is situated along the rotating axis and the rotational motion of the motor shaft is transmitted through ball screws as a linear motion lifting the lower leg.

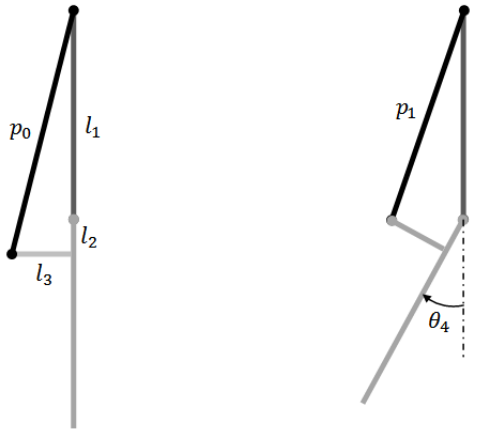

Figure 7. *Knee joint kinematics*

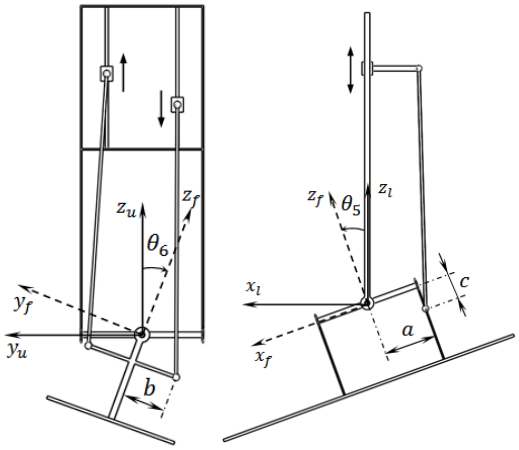

Figure 8. *Ankle joint kinematics Back and Side views*

Conversion of the motor output motion to the linear motion of the nut over the ball screw is determined by the ball screw lead. According to Figure 7, geometric relationships between the linear displacement of the nut and the angular motion of the knee joint are given as follows:

$$\Delta p = p_0 - p_1 = \sqrt{{l_3}^2 + (l_1 + l_2)^2} - \sqrt{{l_1}^2 + {l_2}^2 + {l_3}^2 - 2l_1\sqrt{{l_2}^2 + {l_3}^2}\cos\left(\pi - \tan^{-1}\left(\frac{l_3}{l_2}\right) - \theta_4\right)} \quad (11)$$

$$\frac{\Delta\dot{p}}{\dot{\theta}_4} = \frac{l_1\sqrt{{l_2}^2+{l_3}^2}\sin\left(\pi-\tan^{-1}\left(\frac{l_3}{l_2}\right)-\alpha\right)}{\sqrt{{l_1}^2+{l_2}^2+{l_3}^2-2l_1\sqrt{{l_2}^2+{l_3}^2}\cos\left(\pi-\tan^{-1}\left(\frac{l_3}{l_2}\right)-\theta_4\right)}} \quad (12)$$

where Δp and θ_4 represent respectively the linear displacement over the ball screw and the knee joint angle.

3.1.3. Ankle Joints

Since the ankle joint consists of two rotational DoF, the related general motion is spatial. Derivation of kinematics is basically similar to that of the knee joint.

Let θ_5 and θ_6 represent the angular positions of the foot about the transversal and longitudinal axes of the ankle joint (Figure 8). Three reference frames R_l , R_u and R_f which are located at the center of the

universal coupling at the ankle joint, are respectively fixed to the lower leg, center of the universal joint and foot. $(x_0 \quad y_0 \quad z_0)^T$ and $(x_1 \quad y_1 \quad z_1)^T$ represent the coordinates of the ball joints in R_l. Relative motion of the linear displacement of the nuts gives rise to angular motions around two axes of the ankle joint as shown in Figure 8. The lower ball joints are free to move in space and the higher ball joints are constrained to linear displacements over the ball screw.

Using appropriate coordinate transformations between the reference frames, mathematical relationships governing the ankle kinematics are given as follows:

$$x_0 = a.\cos\theta_5 + b.\sin\theta_5 . \sin\theta_6 + c.\sin\theta_5 . \cos\theta_6 \tag{13}$$

$$y_0 = b.\cos\theta_6 + c.\sin\theta_6 \tag{14}$$

$$z_0 = -a.\cos\theta_5 + b.\cos\theta_5 . \sin\theta_6 + c.\cos\theta_5 . \cos\theta_6 \tag{15}$$

$$z_1 = \sqrt{l^2 - (x_1 - x_0)^2 - (y_1 - y_0)^2} + z_0 \tag{16}$$

$$\dot{x}_0 = -a.\cos\theta_5 . \dot{\theta}_5 + b.\left(\cos\theta_5 . \sin\theta_6 . \dot{\theta}_5 + \sin\theta_5 . \cos\theta_6 . \dot{\theta}_6\right) + c.\left(\cos\theta_5 . \cos\theta_6 . \dot{\theta}_5 + \sin\theta_5 . \sin\theta_6 . \dot{\theta}_6\right) \tag{17}$$

$$\dot{y}_0 = -b.\sin\theta_6 . \dot{\theta}_6 - c.\cos\theta_6 . \dot{\theta}_5 \tag{18}$$

$$\dot{z}_0 = -a.\cos\theta_5 . \dot{\theta}_5 + b.\left(\sin\theta_5 . \sin\theta_6 . \dot{\theta}_5 + \cos\theta_5 . \cos\theta_6 . \dot{\theta}_6\right) + c.\left(-\sin\theta_5 . \cos\theta_6 . \dot{\theta}_5 - \cos\theta_5 . \sin\theta_6 . \dot{\theta}_6\right) \tag{19}$$

$$\dot{z}_1 = \frac{\dot{x}_0.(x_1 - x_0) + \dot{y}_0.(y_1 - y_0)}{z_1 - z_0} + \dot{z}_0 \tag{20}$$

Equations 13-20 represent the linear motion of the nut in terms of the foot angular motions.

3.2. Mechanical Design

The solid model and dimensions of the robot are given in Figures 9 and 10.

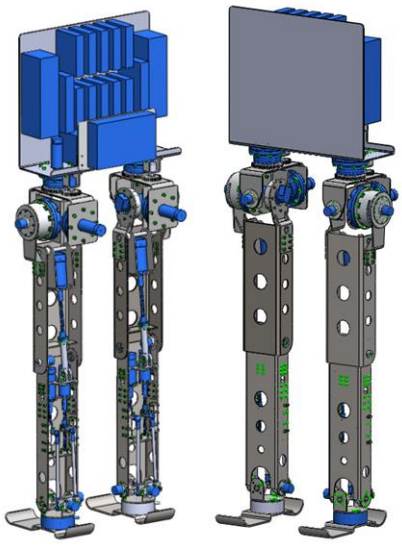

Figure 9. *Solid model of the robot*

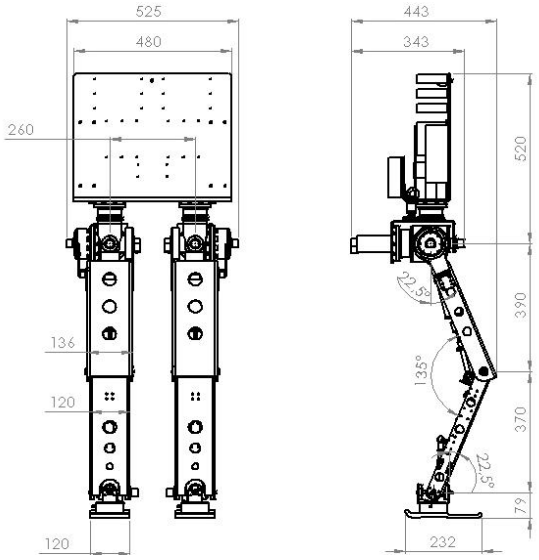

Figure 10. *Dimensions of the robot*

Three rotational DoF at the hip joint are driven by DC motors coupled to compact harmonic drives (Figure 11). Knee and ankle joints are driven by DC motors whose axes are normal to those of joint rotations. The actuators driving the knee and ankle joints are situated higher than the respective rotation axes and the power is transmitted through ball screw mechanisms (Figures 12 and 13).

The ranges of angular motions at the hip joint are limited by $70°$ about the transversal axis, $30°$ about the longitudinal axis and $135°$ about the vertical axis. Rotation axes of the hip joints intersect at one point. Such a configuration allows easier manipulation of the inverse kinematics. The hip DoFs are driven by compact actuation units with Maxon® and Harmonic Drive® components.

The range of the angular motion at the knee joint is limited by $86°$. The ball screw mechanism used for the knee joint acts as a torque amplifier to provide the required conversion ratio.

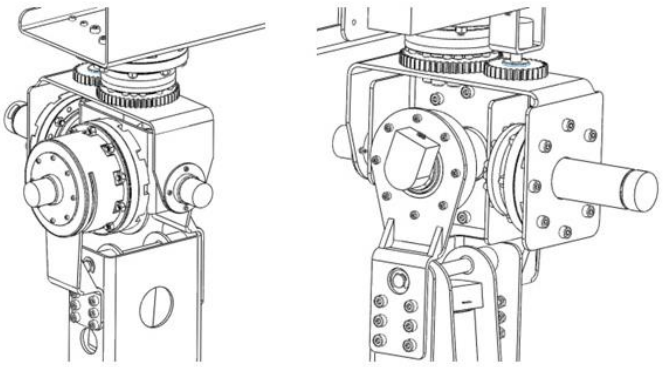

Figure 11. *Hip joint design*

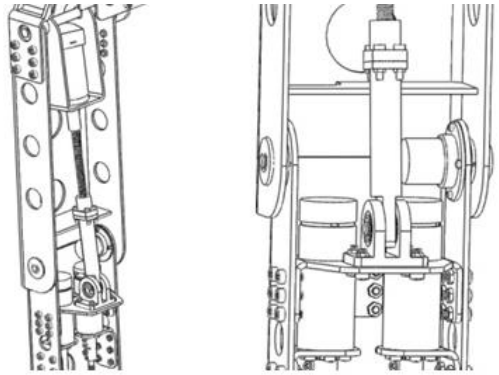

Figure 12. *Knee joint design*

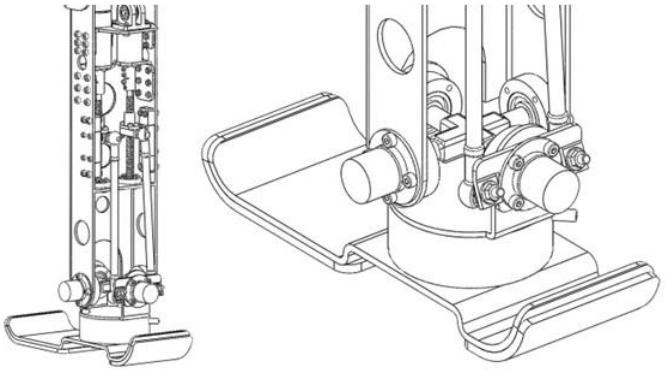

Figure 13. *Ankle joint design*

The actuators situated in the lower legs drive the 2 DoF of the ankle joints whose angular motion ranges are limited by $45°$. 2 DoF of the ankle joints are driven through universal joints placed between the lower legs and feet. The nuts on the ball screw mechanism are guided on a polyamide channel which is mounted on lower leg, limiting the motion of the nuts to linear displacements only. The selected actuators and transmissions are given in Table 1.

Lower and upper legs consist of U-profiles containing all actuation and transmission mechanisms of the knee and ankle joints. An industrial PC with real-time OS, motor drivers and sensor interfaces as well as a battery pack are situated on an upper body upon the hip joints. The entire mechanism has 142 cm tall (136 cm in squad position) and 58 kg weight without batteries.

In such a mechanical design as presented here, the center of mass (CoM) of the robot moves also higher in vertical with respect to that of mechanisms with direct driven joints. This is an important design criterion for biped robots to be controlled through the inverted pendulum approach mentioned in Section 3. The CoM of the robot in squad position is finally situated at 67 cm height from the ground while the motor axes at hip joints intersect at 84 cm.

Table 1. *Actuators and transmissions*

Joint–DoF	**Actuation**	**Transmission**
Hip – x	Maxon® RE-50 (200W)	Harmonic Drive® CSG-25-160
Hip – y	Maxon® RE-50 (200W)	Harmonic Drive® CSG-25-160
Hip – z	Maxon® RE-30 (60W)	Harmonic Drive® CSG-20-100
Knee	Maxon® RE-50 (200W)	Bosch S. Rexroth® 1531-2
Ankle – 1	Maxon® RE-40 (150W)	Bosch S. Rexroth® 1531-1

Ankle – 2	Maxon® RE-40 (150W)	Bosch S. Rexroth® 1531-1

4. CONTROL SYSTEM DESIGN AND INTEGRATION

4.1. Actuators and Sensors

The actuation system of the biped robot consists of 12 Brushed Maxon® RE Series DC motors driven by Maxon EPOS drivers. Power rates of the actuators are given in Table.

The sensory system of the biped robot includes incremental and absolute encoders at all DoFs, two force/torque transducers in the feet and an inertial measurement unit. The Maxon MR L 500 series incremental encoders mounted on the motor shafts measure the angular displacements relative to initial values. Resolution of the incremental encoder which is 2000 increments per revolution satisfies qualified measurement in presence of highly stiff Harmonic Drive gears.

Since incremental encoders measure the differentiation of angular positions, initial angular positions of all joints must be measured by absolute encoders. The Scancon® SCH24AB series absolute encoders which are mounted on the joint shafts are directly connected to the Maxon EPOS drivers. They measure and transmit the initial joint values which are required to initialize the robot in a desired configuration. Measurement errors of the absolute encoders are negligible thanks to its 12-bit resolution per revolution. Besides, 6-axes ATI® MINI85 series F/T transducers are placed in the feet to measure the generalized contact forces which are required for the closed-loop control of the ZMP position.

4.2. Control Hardware

The control hardware scheme is given in Figure 14.

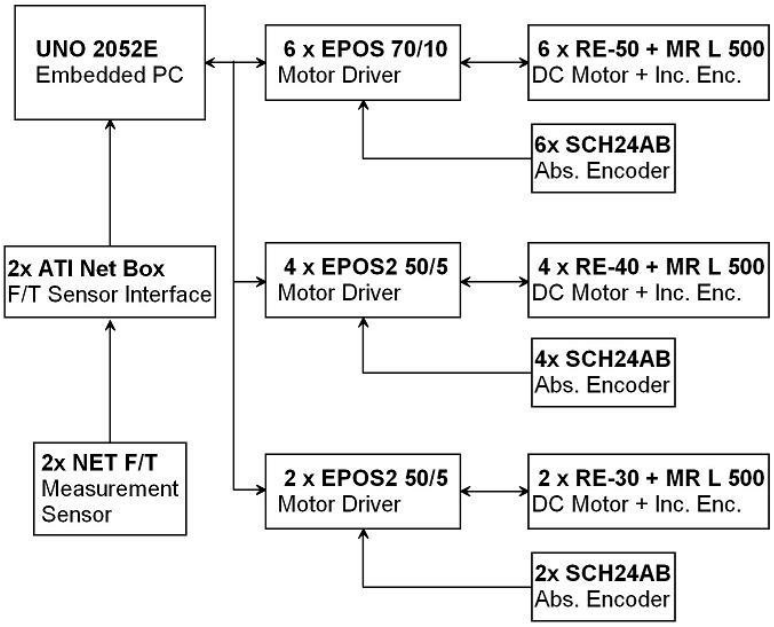

Figure 14. *Control hardware scheme*

The Advantech® UNO 2052E series embedded computer with an AMD GX2-400 MHz processor, 256 MB RAM and 4 GB compact flash card runs a real-time Linux OS. CANbus protocol is used in the data transmission between the embedded computer, motor drivers and force/torque transducers. Trajectory generation, control algorithms and monitoring interfaces are implemented in the embedded PC which can be accessed through cabled or wireless communication. Control programs are coded in C language.

4.3. Construction and Assembly of the Robot

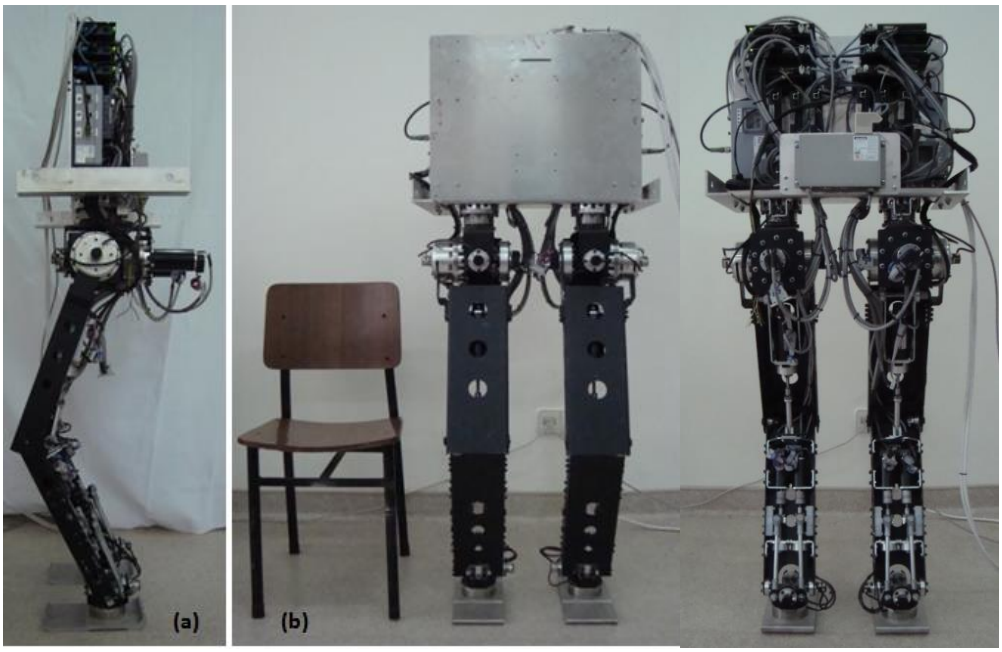

Figure 15. *Side (a), front (b), and back (c) views of the biped robot*

Blue colored components in Figure 9 include the actuators, sensors, computer, battery and related accessories. The biped robot prototype consists of additional 46 pieces of mechanical components, grey colored in Figure 9. Photos of the assembled robot in static equilibrium are given in below Figure 15, showing the side, front and back views of the I.T.U. biped robot. Black colored parts are made by steel and grey colored ones by aluminum.

The compact hip joint with 3 DoF is shown in Figure 16. Figure 17 shows the upper leg and knee joint and Figure 18 lower legs and ankle joints.

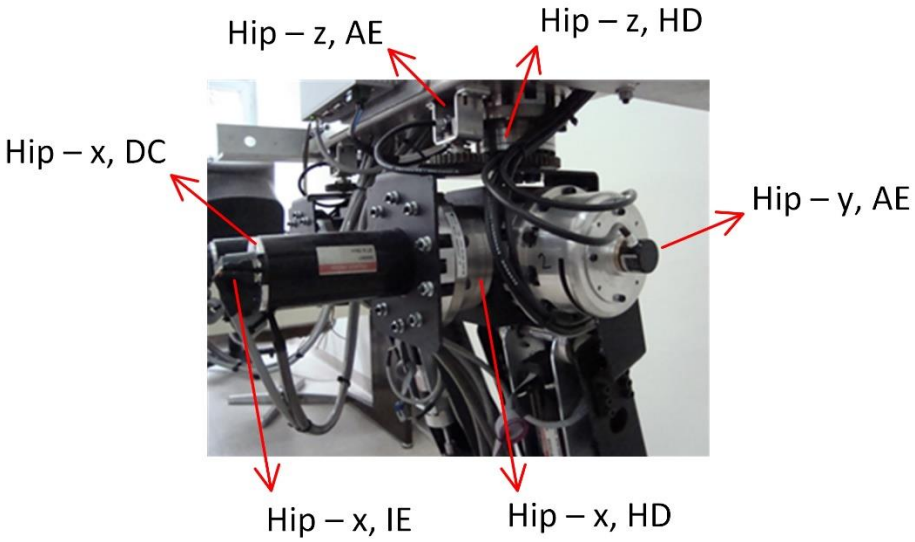

Figure 16. *Side Hip joint detail*

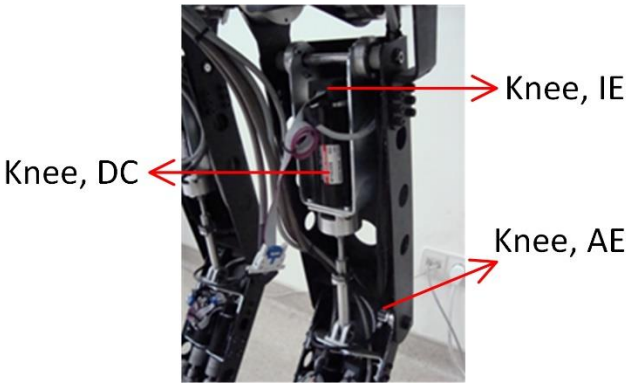

Figure 17. *Upper leg and knee joint*

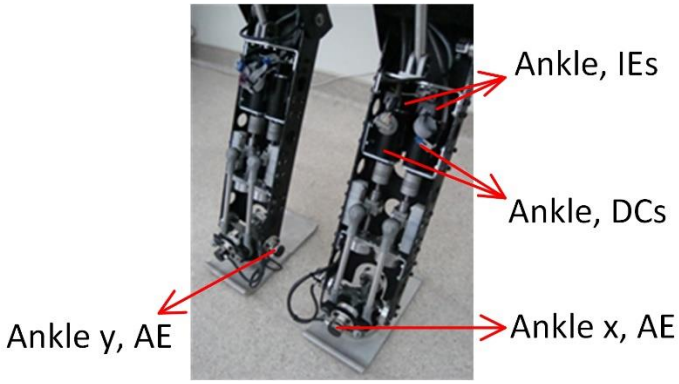

Figure 18. *Lower leg and ankle joint*

5. EXPERIMENTS AND CONCLUSION

5.1. Experiments

The control system has been first tested with the legs swinging on air and synchronized motions of the legs with the joint position references have been successfully controlled. Once on the ground, the stability of the static equilibrium of the robot with its CoM remaining in the support polygon has been experimentally observed.

In the first ground experiments, real-time control of linear motions of the hip along vertical and transversal axes has been achieved. During these motions, ground forces have been permanently measured through the 6-axis F/T transducers and the active joint torque of the robot have been obtained by the following relationship:

$$\boldsymbol{\tau} = \boldsymbol{J}^{\boldsymbol{T}}(\boldsymbol{q})\,\boldsymbol{F} \tag{21}$$

where $\boldsymbol{\tau}$ and $\boldsymbol{F}$ represent respectively the vector of joint torque and vector of external forces due to ground interaction, and $\boldsymbol{J}(\boldsymbol{q})$ is the Jacobian matrix of the leg.

The same joint torque vector has also been computed through the motor currents and transmissions kinematics. At the hip joints where the DoFs are driven by harmonic reducers, the joint torque is easily computed through the motor torque constant and reduction ratio:

$$\boldsymbol{\tau} = \boldsymbol{N}\,\boldsymbol{k_t}\,\boldsymbol{i} \tag{22}$$

where N is the transmission ratio of harmonic reducer, k_t is the motor torque constant and i is the motor current. At the knee and ankle joints, transmission kinematics given in Equations (12-20) in Section 3 are used to compute corresponding joint torque.

A schematic diagram of the control system implemented for the experimentations is given in Figure 19.

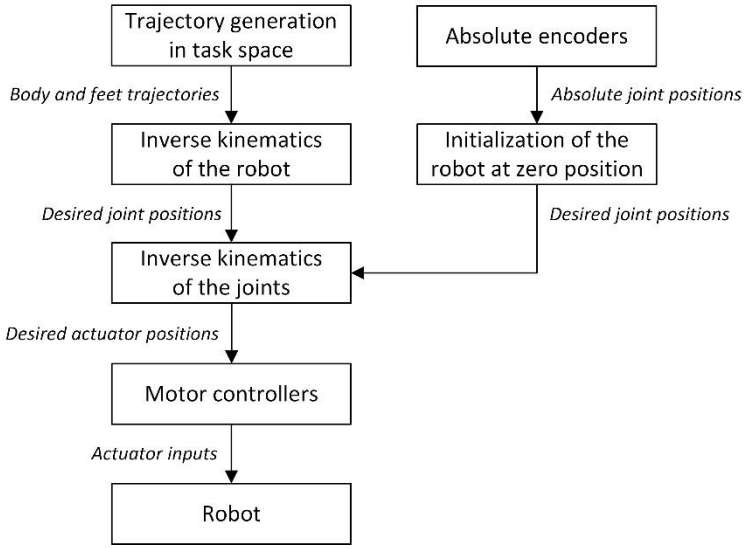

Figure 19. *Control system implemented for experimentations*

5.1.1. Vertical Motion

The reference motion of the robot is the translation of the hip 10cm down and up along the vertical axis (Figure 20). Active joint torque of the robot obtained from the F/T transducers and from the actuator currents are given in Figure 21.

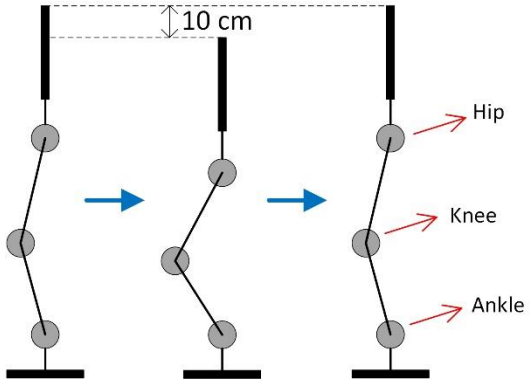

Figure 20. *Side view of the robot in vertical motion*

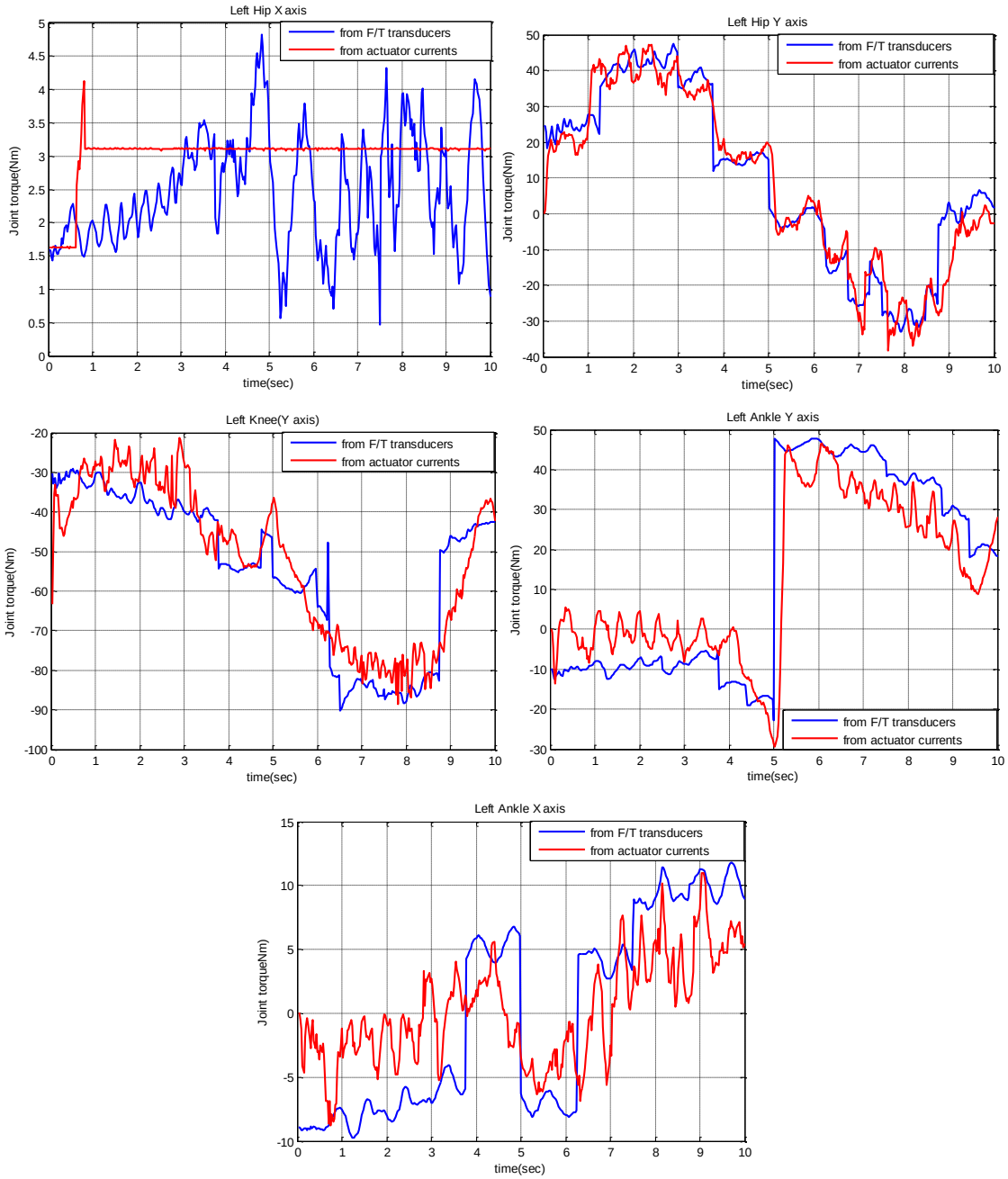

Figure 21. *Joint torque of the left leg in vertical motion of the CoM*

5.1.2. Lateral Motion

The reference motion of the robot is the translation of the hip 13cm right and left along the transverse axis (Figure 22). Joint torque obtained by the above mentioned methods are given in Figures 23 and 24.

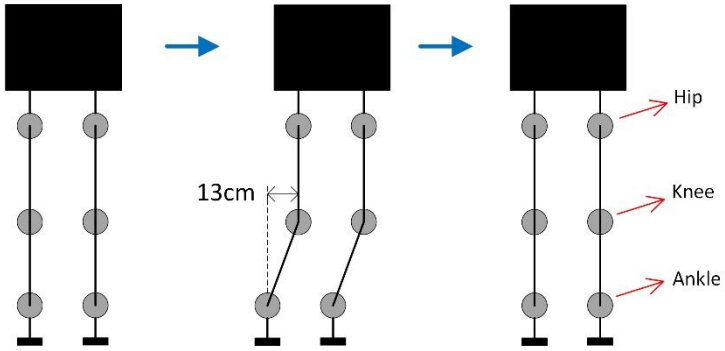

Figure 22. *Front view of the robot in horizontal motion*

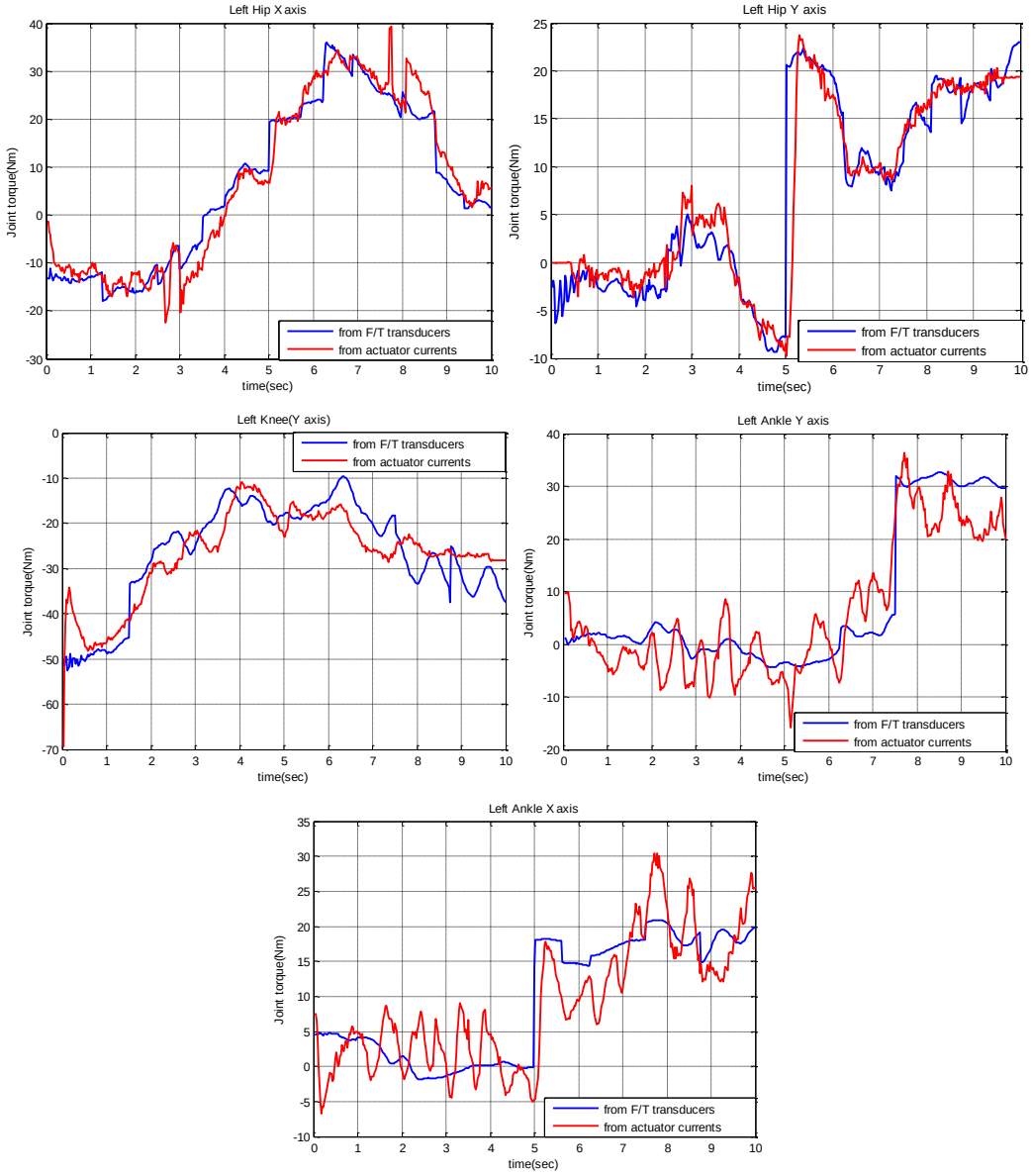

Figure 23. *Joint torque of the left leg in lateral motion of the hip*

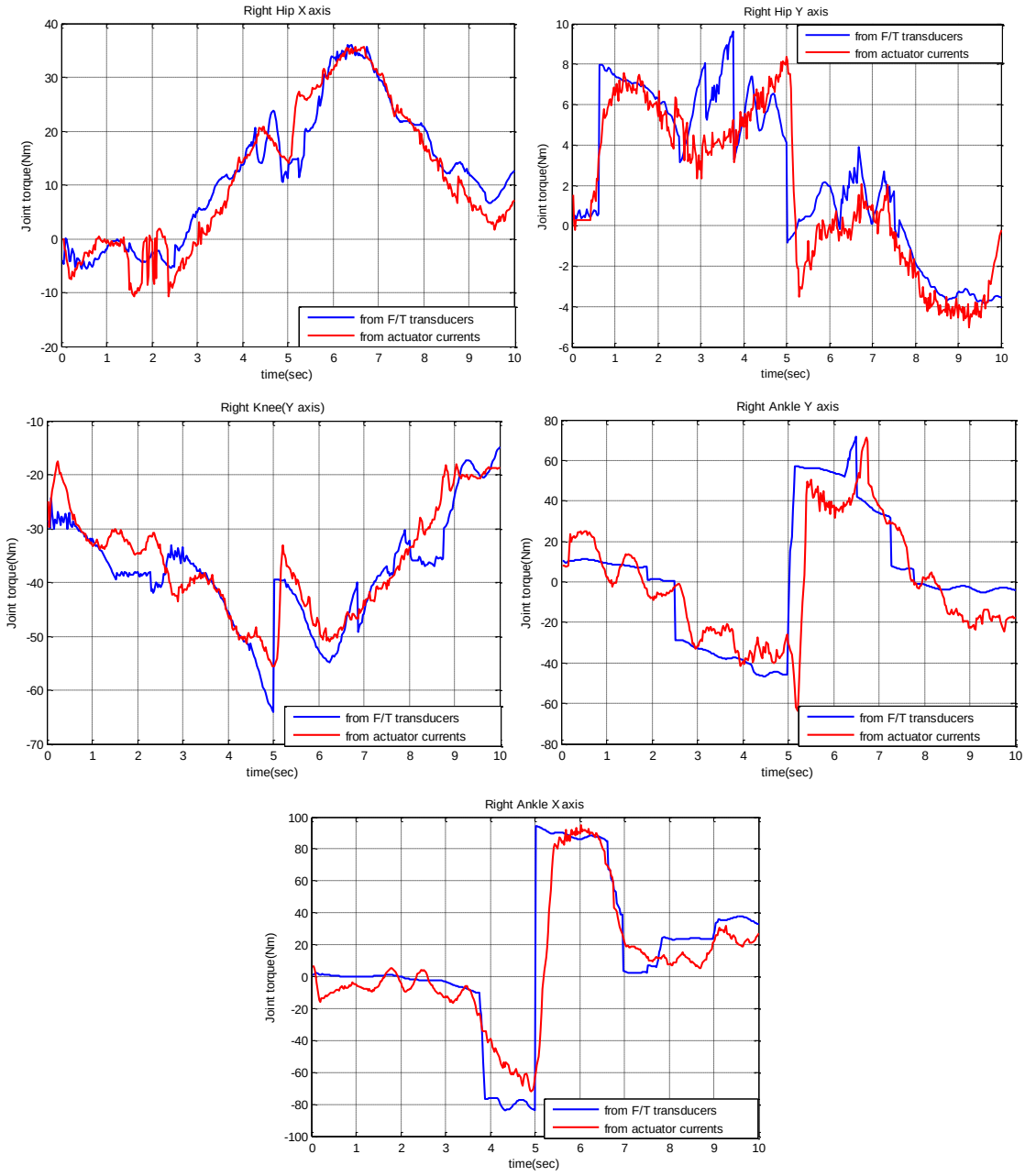

Figure 24. *Joint torque of the right leg in lateral motion of the hip*

Although they display similar trends, Figures 21, 23 and 24 show that the joint torque obtained from the F/T transducers and from actuator currents do not exactly match. In both methods, kinematics equations are used to compute the joint torque: leg kinematics with the F/T transducers and transmission kinematics with the actuator currents. In fact, there are some physical phenomena neglected in kinematics modelling.

The first source of deviation observed in ankle joint torque is due to the elasticity of spherical joints used in ankle transmissions (Figures 8, 13 and 18). The elastic behavior of the spherical joints used in motion transmission is not exactly compatible with the assumption of rigid joint mechanism. Deviations observed in ankle joint torque are mainly due to this modelling imprecision.

Secondly, kinematics models used in modelling of mechanical transmissions do not take into account actuator dynamics. Effects of actuator dynamics happen to be inversely proportional with transmission ratios. Therefore, imprecisions observed in knee and ankle joint torque calculations are partly due to lower transmission ratios with respect to hip joint transmissions established with harmonic reducers.

Finally, the friction effects have been neglected in mathematical models used in computing joint torque. Friction operating at ball bearings is an important source of disturbance for the motion control of robot joints. Disturbance torque due to friction is known to be a complex physical phenomenon, whose mathematical models can be obtained through identification methods only. On the one hand, highly nonlinear behavior of friction effects are especially observed around zero value of joint velocities. Complexity of mathematical modelling is due to the interactions between static, Coulomb (dry) and viscous friction effects. On the other hand, dynamics introduced by friction at low velocities of joints dominate the inertia, centrifugal and Coriolis forces. Therefore, friction effects neglected in kinematics modelling of legs and transmissions appear as a major source of deviation between measured and computed quantities. Deviations become especially dominant where the joint velocities change sign.

Deviations observed in Figures 21, 23 and 24 are mainly due to the cumulated effects of these neglected phenomena. Another practical cause of the observed deviations is related to measurement of force/torque and current variables. Signal noise introduced by the F/T transducers and driver units measuring motor currents contribute to the imprecisions between joint torque obtained through two different method presented in this section.

5.2. Conclusion

Design and development of a new biped robot have been presented in this paper. The entire work consisted of the following steps: Modelling of kinematics and dynamics of the walking biped mechanism; Modelling of biped walking behavior; Design of control system; Dimensioning of the mechanism through dynamic simulations; Mechanical and electrical designs; and Construction of the prototype.

In the first ground experiments, the components of the control system have been fully integrated and the static equilibrium of the robot has been verified. The robot's hip has been given vertical and lateral motion references. During these motions, the joint torque of the robot have been obtained from the F/T transducers and actuator currents. The on-going work consists of the implementation of controllers for stable walking over linear and curvilinear trajectories.

CONFLICTS OF INTEREST

No conflict of interest was declared by the authors.

ACKNOWLEDGEMENTS

This work is funded by TUBITAK (The Scientific and Technological Research Council of Turkey) Research Project No.106M340 and supported by Altinay Robot Technologies, Inc. Zeki Y. Bayraktaroğlu thanks Hikmet Kocabaş for his precious advices in prototype design.

REFERENCES

[1] Hirai, K., "Current and Future Perspective of Honda Humanoid Robot", Proceedings of the IEEE/RSJ International Conference on Intelligent Robots, Grenoble, France, 2: 500–508, (1997).

[2] Hirai, K., Hirose, M., Haikawa, Y., Takenaka, T., "The Development of Honda Humanoid Robot", Proceedings of the IEEE International Conference on Robotics and Automation, Leuven, Belgium, 2: 1321–1326, (1998).

[3] Sakagami, Y., Watanabe, R., Aoyama, C., Matsunaga, S., Higaki, N., Fujimura, K., "The intelligent ASIMO: System overwiew and integration", Proceedings of the IEEE/RSJ International Conference on Intelligent Robots, Lausanne, Switzerland, 3: 2478–2483, (2002).

[4] Inoue, H., Tachi, S., Nakamura, Y., Hiari, K., "Overview of Humanoid Robotics Project of METI", Proceedings of the International Symposium on Robotics, Seoul, Korea, 1478–1482, (2001).

[5] Kaneko, K., Kanehiro, F., Kajita, S., Yokoyama, K., Akachi, K., Kawasaki, T., Ota, S., Isozumi, T., "Design of Prototype Humanoid Robotics Platform for HRP", Proceedings of the IEEE/RSJ International Conference on Intelligent Robots, Lausanne, Switzerland, 3: 2431–2436, (2002).

[6] Hirukawa, H., Kanehiro, F., Kaneko, K., Kajita, S., "Humanoid Robotics Platforms Developed in HRP", Robotics and Autonomous Systems, 48(4): 165–175, (2004).

[7] Akachi, K., Kaneko, K., Kanehira, N., Ota, S., Miyamori, G., Hirata, M., Kajita, S., Kanehiro, F., "Development of Humanoid Robot HRP-3P", Proceedings of the IEEE RAS International Conference on Humanoid Robots, Tsukuba, Japan, 50–55, (2005).

[8] Takanishi, A., Ishida, M., Yamazaki, Y., Kato, I., "The realization of dynamic walking by the biped walking robot WL-10RD", Proceedings of the International Conference on Advanced Robotics, 459–466, (1985).

[9] Lim, H., Takanishi, A., "Biped walking robots created at Waseda University: WL and WABIAN family", Phil. Transactions of the Royal Society A, 365: 49–64, (2007).

[10] Park, I.W., Kim, J.Y., Lee, J., Oh, J.H., "Mechanical design of humanoid robot platform KHR-3", Proceedings of the IEEE RAS International Conference on Humanoid Robots, Tsukuba, Japan, 321–326, (2005).

[11] Pfeiffer, F., Löffler, K., Gienger, M., "The Concept of Jogging JOHNNIE", Proceedings of the IEEE International Conference on Robotics and Automation, Washington D.C., USA, 3129–3135, (2002).

[12] Löffler, K., Gienger, M., Pfeiffer, F., "Sensor and Control Design of a Dynamically Stable Biped Robot", Proceedings of the IEEE International Conference on Robotics and Automation, Taipei, Taiwan, 1: 484–490, (2003).

[13] Lohmeiner, S., Löffler, K., Gieber, M., Ulbrich, H., "Computer System and Control of Biped Johnnie", Proceedings of the IEEE International Conference on Robotics and Automation, New Orleans, USA, 4: 4222–4227, (2004).

[14] Lohmeier, S., Buschmann, T., Ulbrich, H., Pfeiffer, F., "Modular Joint for Performance Enhanced Humanoid Robot Lola", Proceedings of the IEEE International Conference on Robotics and Automation, Orlando, USA, 88–93, (2006).

[15] http://www.pal-robotics.com/ (2012), Pal Robotics Website. Accessed February 2012.

[16] Erbatur, K., Seven, U., Taskiran, E., Koca, O., Yilmaz, M., Unel, M., Kiziltas, G., Sabanovic, A., Onat A., "SURALP: a new full-body humanoid robot platform", Proceedings of the IEEE/RSJ International Conference on Intelligent Robots, Saint Louis, USA, 4949–4954, (2009).

[17] Raibert, M.H., Legged Robots That Balance, MIT Press, Cambridge, (1986).

[18] Wisse, M., Schwab, A., "First steps in passive dynamic walking", Proceedings of the Climbing and Walking Robots, London, UK, VII, 745–756, (2005).

[19] Espiau, B., Sardain, P., "The anthropomorphic biped robot BIP2000", Proceedings of the IEEE International Conference on Robotics and Automation, San Francisco, USA, 4: 3996–4001, (2000).

[20] Konno, A., Sellaouti, R., Ben Amar, F., Ben Ouezdou, F., "Design and Development of the Biped Prototype ROBIAN", Proceedings of the IEEE International Conference on Robotics and Automation, Washington D.C., USA, 1384–1389, (2002).

[21] http://www.bostondynamics.com/ (2012), Boston Dynamics Corp. Website. Accessed February 2012.

[22] Chevallereau, C., Bessonet, G., Abba, G., Aoustin, Y., "Bipedal Robots: Modeling, Design and Walking Synthesis", Wiley-ISTE, (2008).

[23] Gubina, F., Hamami, H., McGhee, R.B., "On the Dynamic Stability of Biped Locomotion", IEEE Transactions on Biomedical Engineering, (21)2: 102–108, (1974).

[24] McGhee, R.B., "Principles of Walking and Running", in Advances in Comparative and Environmental Physiology, 11, Springer-Verlag, Berlin, (1992).

[25] Vukobratovic, M., Borovac, B., Surla, D., Stokic, D., "Biped Locomotion", Springer-Verlag, Berlin, (1990).

[26] Potkonjak, V., Vukobratovic, M., Babkovic, K., Borovac, B., "Human and Humanoid Dynamics", Journal of Intelligent and Robotic Systems, 41: 65–84, (2004).

[27] Vukobratovic, M., Potkonjak, V., Tzafestas, S., "General Model of Dynamics of Human and Humanoid Motion: Feasibility, Potentials and Verification", International Journal of Humanoid Robotics, 3(1): 21–47, (2006).

[28] Takanishi, A., Hun-ok, L., Tsuda, M., Kato, I., "Realization of Dynamic Biped Walking Stabilized By Trunk Motion on a Sagittally Uneven Surface", Proceedings of the IEEE International Workshop on Intelligent Robots and Systems, 1: 323–330, (1990).

[29] Yamaguchi, I., Takanishi, A., Kato, I., "Development of a Biped Walking Robot Compensation for Three-Axis Moment by Trunk Motion", Proceedings of the IEEE/RSJ International Conference on Intelligent Robots, Tokyo, Japan, 192–200, (1993).

[30] Shih, C.L., Li, Y.Z., Churng, S., Lee, T.T., Gruver, W.A., "Trajectory Synthesis And Physical Admissibility For A Biped Robot During The Single-Support Phase", Proceedings of the IEEE International Conference on Robotics and Automation, Cincinnati, USA, 3: 1646–1652, (1990).

[31] Shih, C.L., Gruver, W.A., "Control of a Biped Robot in the Double-Support Phase", IEEE Transactions on Systems Man and Cybernetics, 22: 729–735, (1992).

[32] Shih, C.L., Gruver, W.A., Lee, T.T., "Inverse Kinematics and Inverse Dynamics for Control of Biped Walking Machine", Journal of Robotic Systems, 10(4): 531–555, (1993).

[33] Shih, C.L., "The dynamics and control of a biped walking robot with seven degrees of freedom", ASME Journal of Dynamical Systems Measurement and Control, 118: 683–690, (1996).

[34] Kajita, S., Yamaura, T., Kobayashi, A., "Dynamic Walking Control Of A Biped Robot Along A Potential Energy Conserving Orbit", IEEE Transactions on Robotics and Automation, 8(4): 431–438, (1992).

[35] Kajita, S., Kanehiro, F., Kaneko, K., Fujiwara, K., Yokoi, K., Hirukawa, H., "Biped walking pattern generation by a simple three-dimensional inverted pendulum model", Advanced Robotics, 17(2): 131–147, (2003).

[36] Kajita, S., Kanehiro, F., Kaneko, K., Fujiwara, K., Harada, K., Yokoi, K., Hirukawa, H., "Biped Walking Pattern Generation by using Preview Control of Zero-Moment Point", Proceedings of the IEEE International Conference on Robotics and Automation, Taipei, Taiwan, 2: 1620–1626, (2003).

[37] Park, J.H., Kim, K.D., "Biped Robot Walking using Gravity-Compensated Inverted Pendulum Mode and Computed Torque Control", Proceedings of the IEEE International Conference on Robotics and Automation, Leuven, Belgium, 3528–3533, (1998).

[38] Park, J.H., Youm, Y., "General ZMP Preview Control for Bipedal Walking", Proceedings of the IEEE International Conference on Robotics and Automation, Roma, Italy, 2682–2687, (2007).

[39] Choi, Y., You, Y.J., Oh, S.R., "On the Stability of Indirect ZMP Controller for Biped Robot Systems", Proceedings of the IEEE/RSJ International Conference on Intelligent Robots, Sendai, Japan, 2: 1966–1971, (2004).

[40] Choi, Y., Kim, D., You, Y.J., "On the Walking Control for Humanoid Robot based on Kinematic Resolution of CoM Jacobian with Embedded Motion", Proceedings of the IEEE International Conference on Robotics and Automation, Orlando, USA, 2655–2660, (2006).

[41] Choi, Y., Kim, D., Oh, Y., You, Y.J., "Posture/Walking Control for Humanoid Robot Based on Kinematic Resolution of CoM Jacobian With Embedded Motion", IEEE Transactions on Robotics and Automation, 23(6): 1285–1293, (2007).

[42] Acar, M., Gercek, A., Tasasiz, B., Bayraktaroglu, Z.Y., Kocabas, H., "Design of a 12-DoF Biped Robot", Proceedings of the International Conference on Recent Achievements in Mechatronics, Automation, Computer Science and Robotics, Tirgu-Mures, Romania, 215–226, (2010).

[43] Luh, J.Y.S., Walker, M.W., Paul, R.P.C., "On-line Computational Scheme for Mechanical Manipulators", ASME Journal of Dynamical Systems Measurement and Control, 102(2): 69–76, (1980).